Chapter 6

Impact of 13-93 bioactive glass addition on the structural, mechanical, *in-vitro* degradation, cell culture, and antibacterial response of the ZTA-based biocomposite materials

6.1 Introduction

The primary criteria for an artificial replacement in addressing a bone defect are mechanical strength and osteoconductivity. Monolithic structural ceramics, specifically alumina (Al_2O_3) and zirconia (ZrO_2) are widely employed due to their superior attributes compared to traditional metallic implants. The notable advantages include their ability to avoid releasing toxic elements in the body, resistance to corrosion, and strong mechanical strength. These qualities have led to the remarkable success of Al_2O_3 and ZrO_2 in the field of orthopedic implants (Lee *et al.*, 2021) (Ortmann *et al.*, 2012). However, there have been documented instances of individual Al_2O_3 and ZrO_2 implants experiencing failures *in-vivo* (Piconi *et al.*, 1999) (Turon-Vinas *et al.*, 2018) (Fan *et al.*, 2017) (Kohorst *et al.*, 2012). In this context, zirconia toughened alumina (ZTA) is developed to address the limitations by combining the Al_2O_3 and ZrO_2. ZTA exhibits enhanced mechanical properties by integrating the remarkable fracture toughness of ZrO_2 with the excellent hardness of Al_2O_3 (Fan *et al.*, 2017). Additionally, the random distribution of ZrO_2 particles within the dense Al_2O_3 matrix reduces the sluggish crack formation generally found in the aging process of ZrO_2 (Fan *et al.*, 2017). Despite its superior mechanical characteristics, ZTA lacks osteoconductivity, a second crucial requirement for implants (Rahaman *et al.*, 2007). ZTA's inert nature limits bonding and integration with host tissue (Roualdes *et al.*, 2010) (Li *et al.*, 2012) (Pezzotti *et al.*, 2017) (Fabbri *et al.*, 2014) (Kurtz *et al.*, 2014) (Rahaman *et al.*, 2007). Surface roughening methods like grinding and sandblasting are suggested to improve implant integration with host tissue by encouraging cell adhesion and bone formation. However, with these methods, implants are loosened, and the formation of biofilms takes place (Wennerberg, 1998) (Kosmač *et al.*, 1999).

As a substitute approach, attempts have been undertaken to improve surface functionality by adding hydroxyl (-OH) groups. It has been found that these surface hydroxyl groups act as nucleation sites where bone-like apatite can form. In alignment with this concept, efforts are

made to hydroxylate the surfaces of Al_2O_3 and ZrO_2 ceramics through immersion in acidic or basic solvents (Fischer *et al.*, 2005) (Miyazaki *et al.*, 2002) (Niedhart *et al.*, 2004) (Böke *et al.*, 2014). Many researchers also tried to encourage the apatite-forming capability of Al_2O_3-ZrO_2 composites through chemical surface treatment (Uchida *et al.*, 2001) (Dehestani *et al.*, 2013) (Faga *et al.*, 2012). However, long-term immersion carries a high risk of surface roughening and etching, which could result in the development of biofilms (Uchida *et al.*, 2001) (Dehestani *et al.*, 2013) (Faga *et al.*, 2012). Apart from immersion in acidic or basic solvents, some other methods are also employed to enhance the bonding between implants and host tissue, such as surface coating, biomimetic mineralization, and the integration of bioactive materials like hydroxyl apatite (HA), calcium phosphate (CaP), and bio-glasses (BG) (Dehestani *et al.*, 2012). Bioactive glass enhances the bioactivity and cellular response of stabilized ZrO_2 systems (Habibe *et al.*, 2009).

Building on prior research endeavors, the current research objectives are to synthesize a zirconia-toughened alumina-based bio-glass (ZTA-BG) composite. The variations of compositions and sample identification are given in Table 3.3. In this chapter, the effect of 13-93 BG additions on the structural, mechanical, *in-vitro* degradation, cell culture, and antibacterial response of ZTA-BG-based bioceramic composite materials are evaluated.

6.2 Results and discussion

6.2.1. Particle size, XRD, SEM, and FTIR analysis of the prepared precursor

The DLS technique is employed to examine the volume-based particle size distribution of prepared ZTA powders. The results show that the average particle size of the ZTA is around 713±162 nm, as indicated in Fig. 6.1(a). The XRD spectra of ZTA powder calcined at 1200°C is shown in Fig. 6.1(b). Results indicate that mainly alpha-Al_2O_3 and the tetragonal phase of zirconia (*t*-ZrO_2) are observed. The microstructure of the prepared ZTA ceramic powders is

given in Fig. 6.1(c). The ZTA powder indicates the presence of small and sparsely agglomerated particles. Fig. 6.1(d) represents the FTIR spectra of ZTA ceramics. The major characteristic bands are located at 592, 640, 1390, and 2993 cm^{-1}. The characteristic transmittance bands for Zr–O bonds appear at 592 cm^{-1} (Kosmač *et al.*, 1999). The band 640 cm^{-1} corresponds to ZrO_2 (hydroxyl group) (Fischer *et al.*, 2005). The characteristic bands located at 1390 cm^{-1} are caused by the adsorbed CO_2 from the air (Miyazaki *et al.*, 2002) (Niedhart *et al.*, 2004). The characteristic band located at 2966 cm^{-1} is formed by the -C-H bonds (Pezzotti *et al.*, 2017).

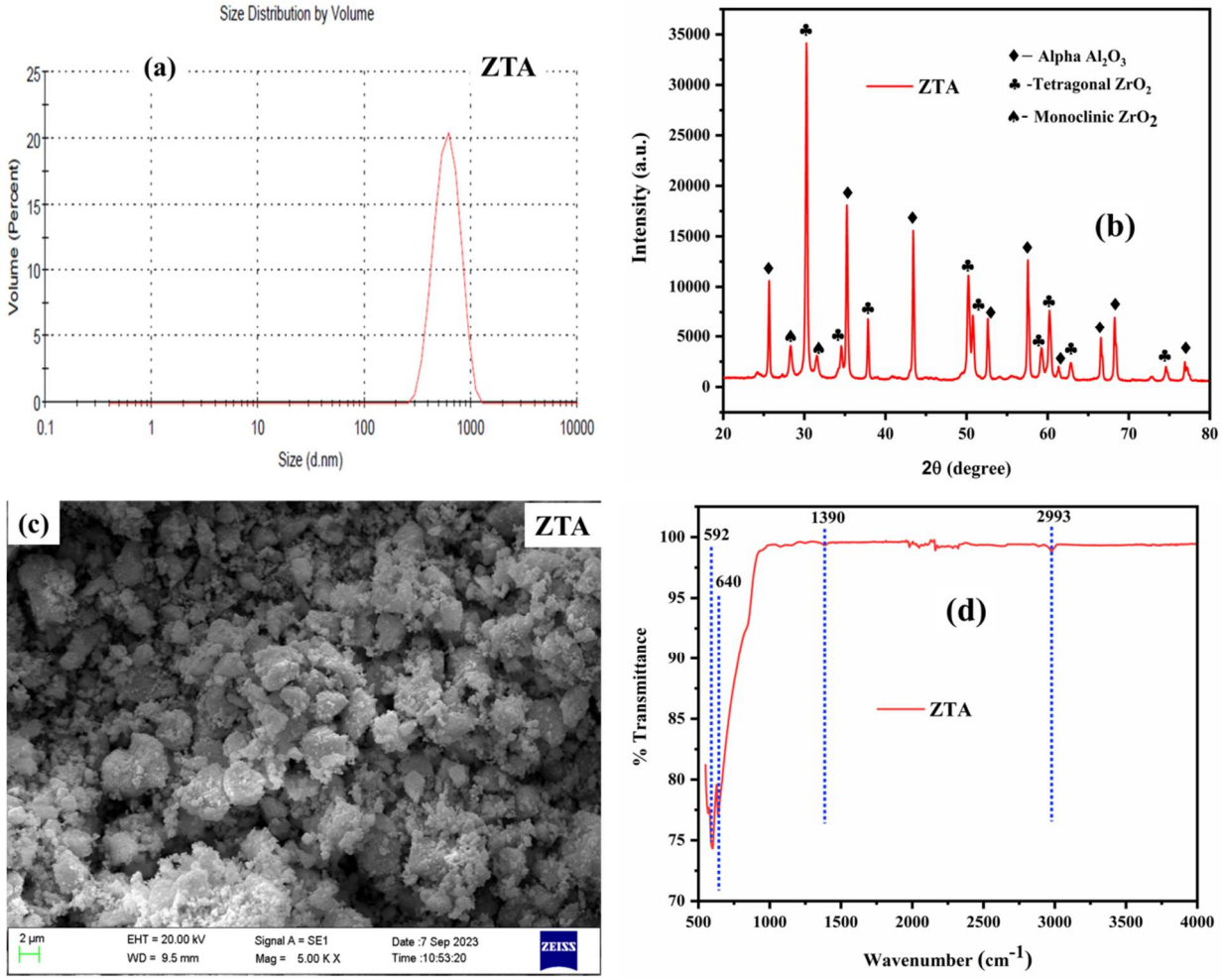

Fig. 6.1 Characterization of the prepared ZTA powders, (a) Particle size distribution (b) XRD, (c) SEM images, and (d) FTIR.

Fig. 6.2 shows the XRD spectra of ZTA powder calcined at different temperatures from 600°C to 1300°C for 4 hrs. The result shows that up to 800°C, ZTA appears amorphous in nature and starts to crystallize at 1000°C. Similarly, amorphous Al_2O_3 starts to crystallize alpha-Al_2O_3 at 1200°C. The major phases present in the XRD pattern are *t*-ZrO_2 (reference code (98-002-7991) and alpha-Al_2O_3 (reference code (98-011-0106). There is also *m*-ZrO_2 (reference code: 98-009-6104) present as a minor phase. Further, the intensity of the *t*-ZrO_2 phases is increased with the calcination temperature. The XRD pattern of the ZTA calcined at 1300°C for 4 hrs shows similar phases to those observed at 1200°C. So, the optimized calcination temperature of ZTA ceramics is 1200°C. The characterization of BG is explained in Section 4.2.1.

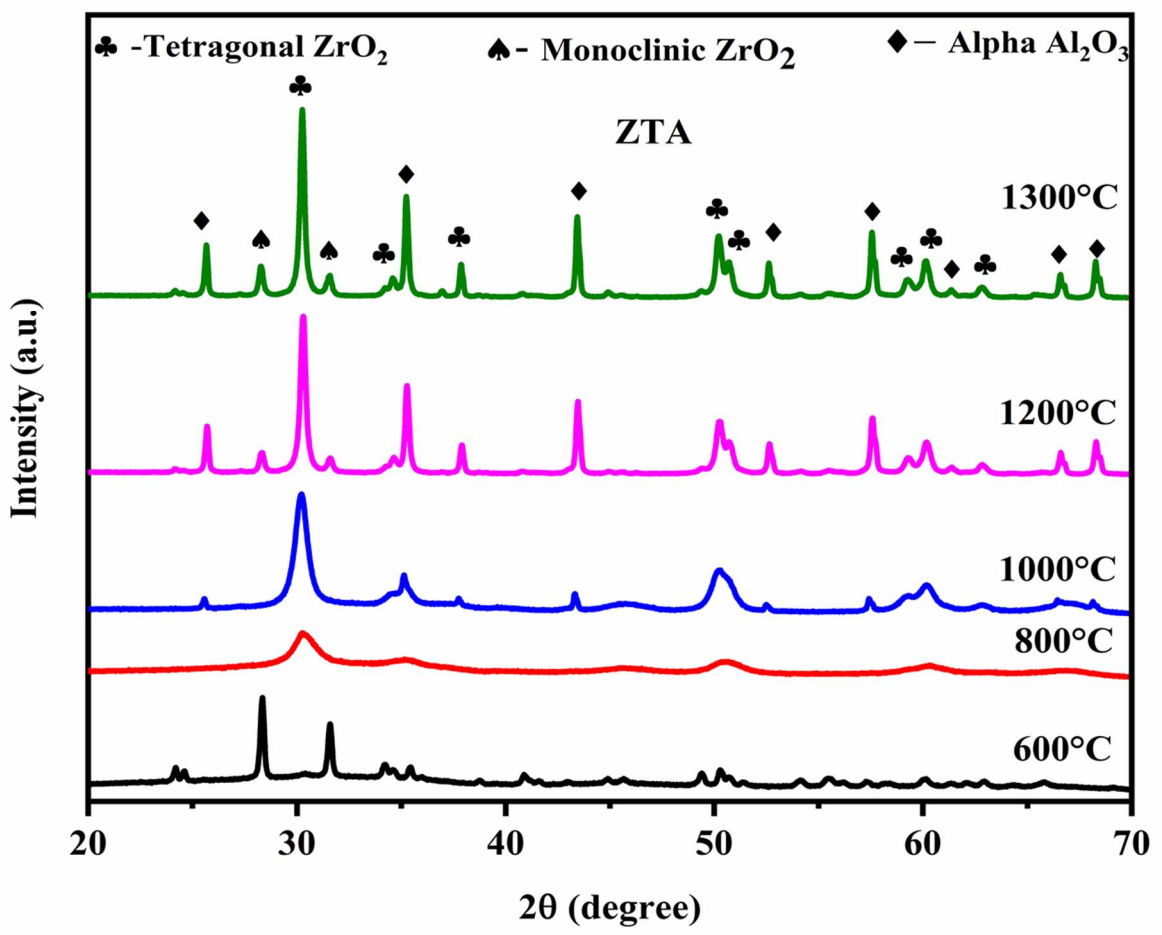

Fig. 6.2 XRD patterns of the prepared powder of ZTA calcined at different temperatures.

6.2.2 XRD and microstructural analysis of the sintered composites

Further, XRD patterns of all composite samples (ABG0, ABG5, ABG10, ABG15, and ABG25) sintered at 1250°C for 4 hrs are represented in Fig. 6.3(a-b). The results reveal that along with alpha-Al_2O_3, *m*-ZrO_2 and *t*-ZrO_2 phases, some additional phases, such as gehlenite ($Ca_2Al_2SiO_7$; reference code: 98-001-1999), nepheline ($KNa_3Al_4Si_4O_{16}$; reference code: 98-001-1935), and akermanite ($Ca_2MgSi_2O_7$; reference code: 98-008-1713) are also observed. It is also noticed that the intensity of the alpha-Al_2O_3 and *t*-ZrO_2 peaks decreases with the increase in BG content. Gehlenite, nepheline, and akermanite are osteoinductive bioceramic materials that can encourage bone repair. The microstructure of ZTA-based biocomposite (ABG0, ABG5, ABG15, and ABG25) sintered at 1250°C for 4 hrs are shown in Fig. 6.4(a-d). The result indicates the loosely arranged grains in a pure ZTA sample. This loosening of the grains (Fig. 6.4(a)) confirms that ZTA has not achieved full densification at 1250°C. The previously reported research papers also proposed that full densification was achieved by pure ZTA ceramics at around 1600°C (Ganesh *et al.*, 2011).

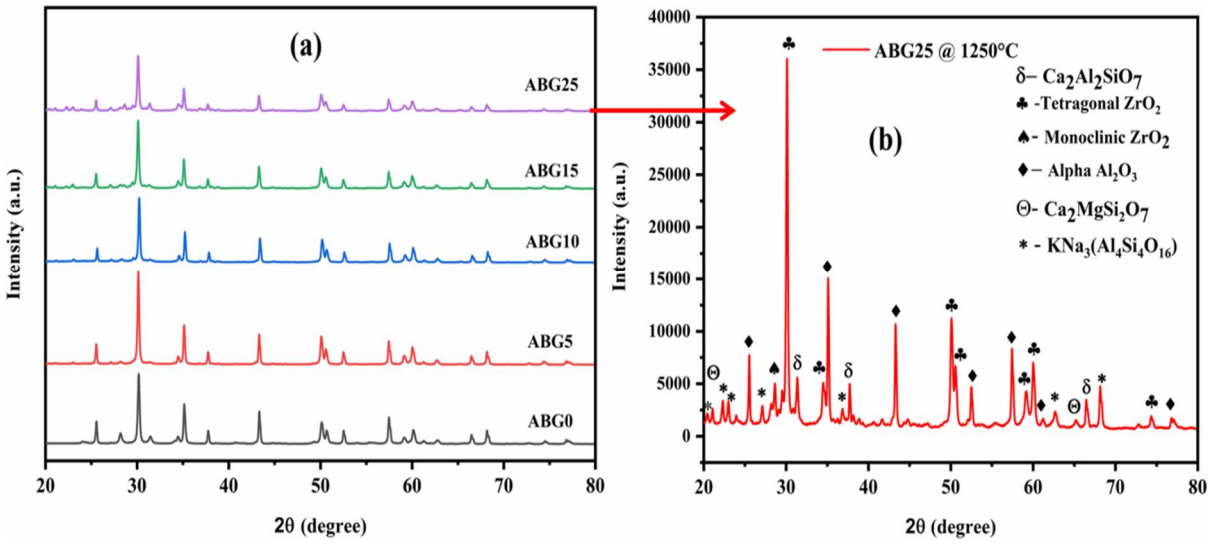

Fig. 6.3 (a) XRD patterns of the composite materials sintered at 1250°C, (b) XRD pattern of ABG25 composite sintered at 1250°C.

Further, Fig. 6.4(b) shows the microstructure of the sample containing 5% BG and indicates that there is an improvement in the sintering process due to the addition of BG particles. Further, the microstructure of the samples containing 10-15wt% of BG indicates that the BG grains are partially crystallized, resulting in the widening of intergranular spaces. The grains are partially shifted from a polygonal shape to a rounder shape as the Al_2O_3 and ZrO_2 dissolve. This indicates a change in the sintering behavior of the samples. Further, the microstructure of the ABG25 sample shows that the maximum grains are converted into a round shape. During the sintering process, the flow becomes viscous with the BG addition. The hypothetical basis of liquid phase sintering clearly indicates that the turbulent flow greatly moistens the minuscule spaces between the solid particles, increasing the capillary pressure in those areas (Ho *et al.*, 2011).

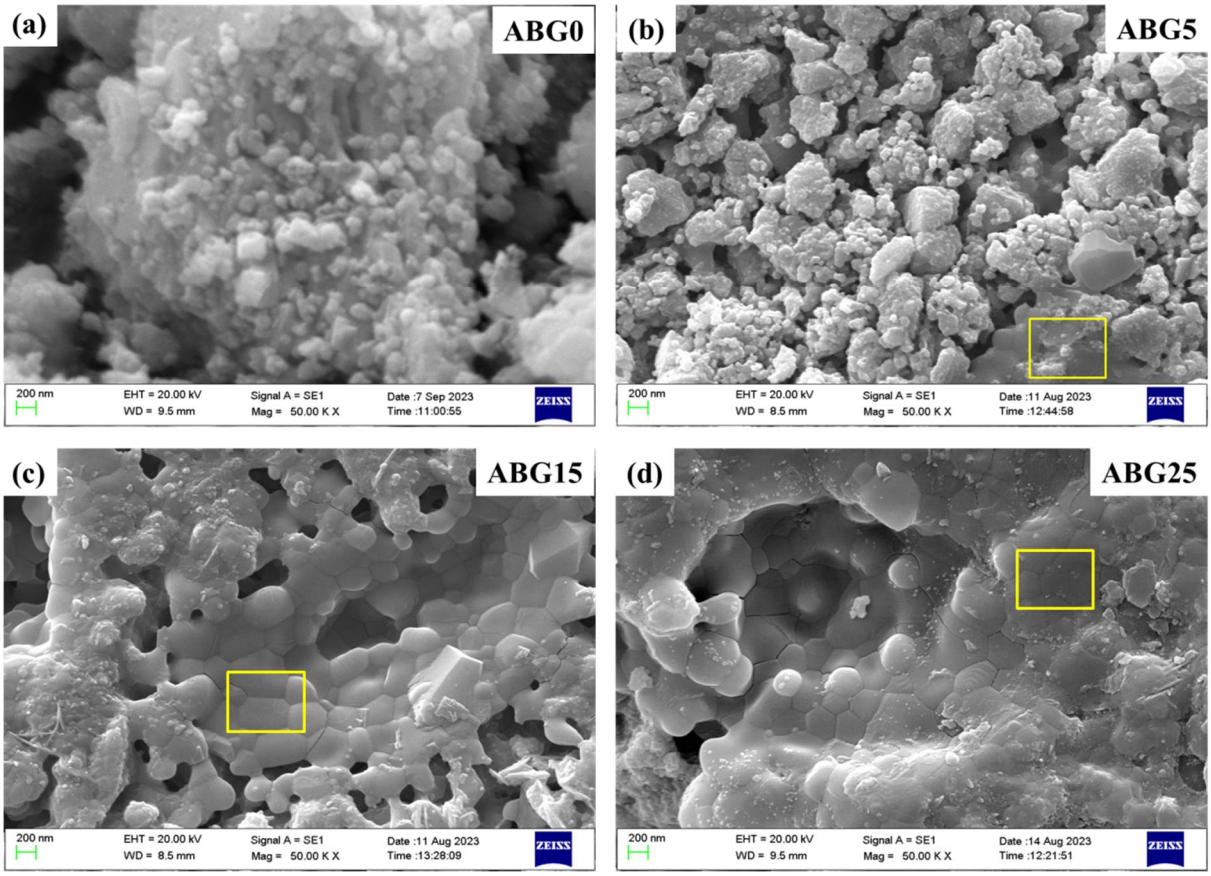

Fig. 6.4 (a-d) SEM images of ZTA-based bioceramic composite materials sintered at 1250°C.

Due to the dispersion of BG particles, it enhances the sample compaction. This compaction is due to the development of a quick diffusion path between ZTA and BG.

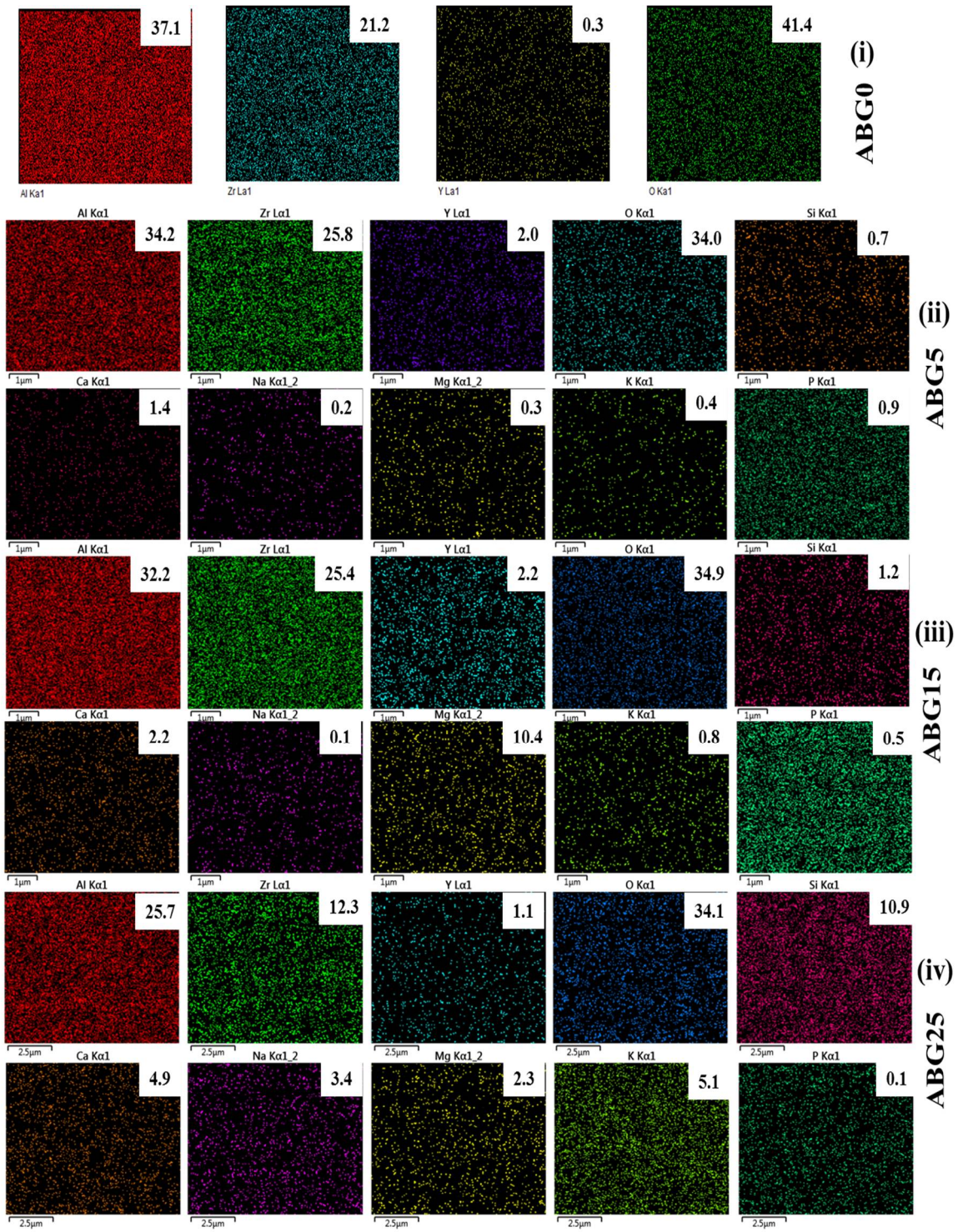

Fig. 6.5 (i-iv) Elemental mapping of bioceramic composite with different BG concentrations (0%, 5%, 15%, and 25%) at 1250^{o}C.

Where mass movement occurs through a dissolution-reprecipitation process and promotes densification. The microstructure images show that the BG component induces a viscous flow during the sintering process, even in the lack of evidence for reprecipitation. The crystalline grains of ZTA are partially wetted with BG frits at 1250^{o}C and compacted with each other. A thin intergranular glassy phase (marked by a yellow square) is observed along the grain boundaries of ZTA within the surface layers. The ZTA grains and the intergranular phases from the BG show a smooth integration. The elemental analysis of the samples (ABG0, ABG5, ABG15, and ABG25) is given in Fig. 6.5(i- iv). Because of the BG concentration, a number of elements are found in the composite, including Al, Zr, Y, Si, Ca, Na, Mg, K, P, and O. It additionally ensures that all the components are distributed uniformly and that no extraneous contaminants are added. The findings indicate that the weight fraction of the Al and Zr elements decreases as the BG concentration rises.

6.2.3 Density and mechanical properties of sintered composites

The experimental, theoretical, and relative densities of all the samples (ABG0, ABG5, ABG10, ABG15, and ABG25) sintered at 1250^{o}C for 4 hrs are shown in Table 6.1. The theoretical densities of all samples are calculated by using the rule of mixture. The values of theoretical density for ZTA and 13-93 bio-glass are 4.43 g/cm^3 and 2.70 g/cm^3, respectively. The results indicate that the experimental and relative densities decrease with increasing the BG concentration, except for the ABG25 sample. The experimental and relative densities are reduced due to the intergranular glassy phase (Ganesh *et al.*, 2011) (de Paula *et al.*, 2019).The reason for the improvement of densification of a sample containing a high amount of BG (ABG25) is due to the increased compactness of structure by easy infiltration of BG due to reduced viscosity sintered at 1250^{o}C.

Table 6.1 Theoretical density, experimental density, relative density, porosity, flexural strength, and hardness of ZTA-based composite materials sintered at 1250°C.

S. No.	Sample Code	Theoretical density (gm/cc)	Experimental density (gm/cc)	Relative density (%)	Porosity (%)	Flexural strength (MPa)	Hardness (GPa)
1.	ABG0	4.43	3.98±0.07	89.84±0.7	10.16	130±11	2.07±0.7
2.	ABG5	4.29	3.57±0.04	83.21±0.9	16.79	141±10	2.17±0.8
3.	ABG10	4.16	2.99±0.06	71.87±0.6	28.13	158±15	2.30±0.6
4.	ABG15	4.04	2.90±0.03	71.78±0.7	28.22	168±19	2.70±0.3
5.	ABG25	3.81	2.93±0.05	76.90±1.0	23.10	197±18	3.02±1.0

The flexural strength and hardness of the ZTA-BG composites are displayed in Table 6.1. The results reveal that both are enhanced by increasing the BG content. Since ZTA and ZTA-based BG composites are sintered at 1250°C for 4 hrs, which is a much lower sintering temperature. At lower sintering temperatures, the improvement in flexural strength and hardness is due to the increased compactness of structure in the composite sample by incorporation of BG particles into ZTA (Ganesh *et al.*, 2011) (de Paula *et al.*, 2019). At this sintering temperature, the viscosity of BG is reduced and infiltrated into the matrix easily. It wets the ZTA and compacts the structure (Ganesh *et al.*, 2011) (de Paula *et al.*, 2019). According to SEM observations, the intergranular space is widened in high BG-contained (15 wt% and 25 wt%) samples, as represented in Fig. 6.4(c & d). The BG frits can easily be incorporated into the matrix by moistening and improving their mechanical properties. Overall, the mechanical properties improve when BG reinforcements are included at lower sintering temperatures.

6.2.4 Biodegradation and bioactivity study

6.2.4.1 pH study

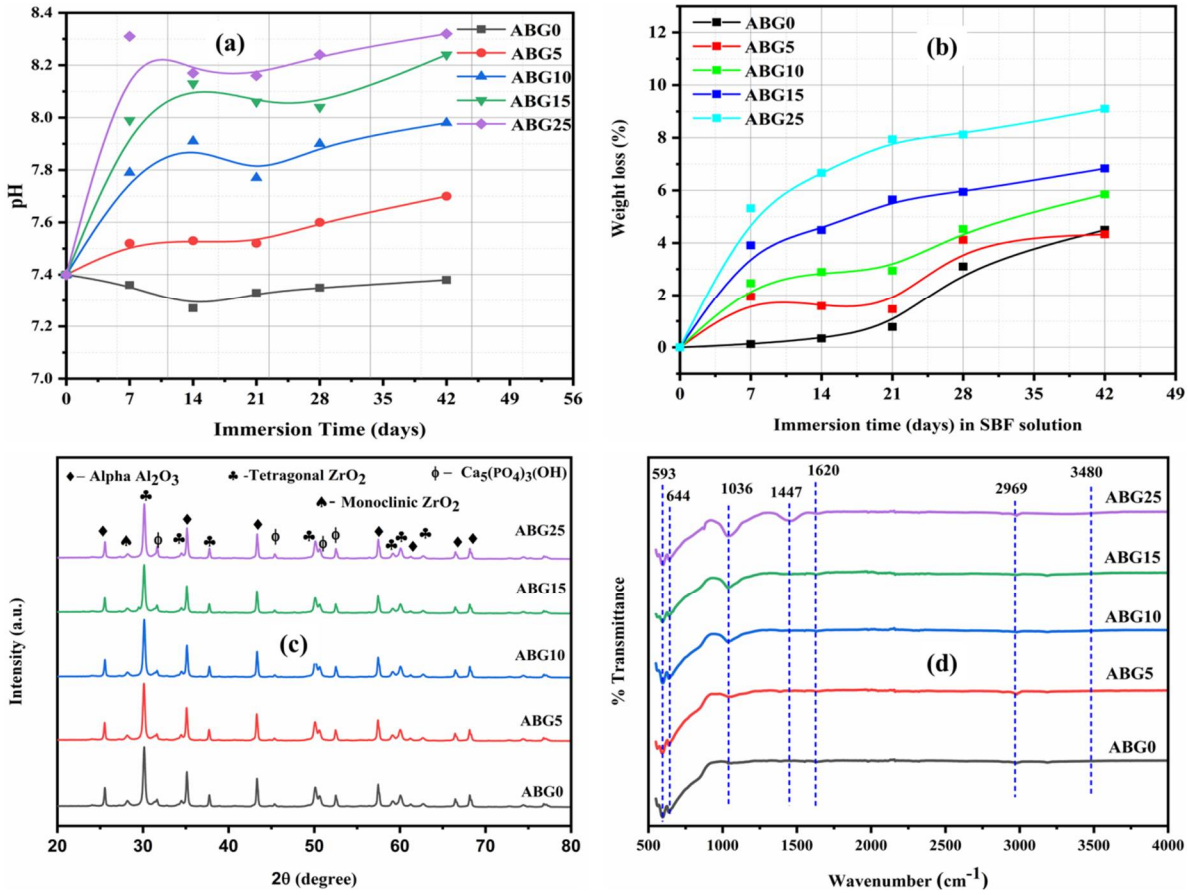

Fig. 6.6 (a) pH measurement with different time intervals, (b) *In-vitro* biodegradability analysis, (c) XRD patterns after 42 days of immersion in SBF, (d) FTIR spectra after 42 days of immersion in SBF.

Fig. 6.6 (a) shows the pH variation in values of all the ZTA-based BG composite samples after soaking in SBF for 7, 14, 21, 28, and 42 days. The initial pH of SBF is reserved constant at 7.4 for every sample. A result indicates that the pH-variation trends significantly depend on immersion time in SBF and BG concentration. The pH value is increased up to 42 days for all samples. The change in the pH is caused by the interactions of ions (such as Na^{+}, Ca^{+}, K^{+}, etc.) in the samples with cations of SBF (H^{+} or H_3O^{+}). During immersion in SBF, the composite sample generates a PO_4^{3-} that draws Ca^{+2} ions present in SBF (Ponnilavan *et al.*, 2019). The Ca^{2+} and PO_4^{3-}ion present in the samples form an apatite layer over the surface of composite samples. Once the apatite layer is formed, pH variation trends are almost constant or lowered for further immersion time (Yadav *et al.*, 2020).

6.2.4.2 Biodegradation analysis

Bio-degradation is an essential aspect of biocomposite. An appropriate amount of elements (Ca^{2+}, P^{5+}, and Si^{4+}) is critical for osteogenesis (Hoppe *et al.*, 2003). Silicate-based biological materials usually degrade by dissolving in SBF (Vyas *et al.*, 2015). In the present study, the BG additive controls the rate of biocomposite degradation, as illustrated in Fig. 6.6(b). The findings demonstrate that the % W_L increases with soaking time and follows an almost uniform trend after that. Degradation is the consequence of an ion exchange between the material and the SBF solution (Zhang *et al.*, 2022). Additionally, it increases as more BG inclusion is added. The decrease in experimental density with BG content could be the one cause of the degradation of materials in SBF. Biodegradation is encouraged by the lower densification and high porosity. As porosity existence helps in ionic interaction between the sample and the surrounding SBF, it speeds up the dissolving process (Devi *et al.*, 2017) (Sarkar *et al.*, 2019).

6.2.4.3 Bioactivity analysis

The *in-vitro* bioactivity is studied of all the samples (ABG0, ABG5, ABG10, ABG15, and ABG25) after soaking for 7, 14, 21, 28, and 42 days of submersion in SBF. However, only the best result of bioactivity is shown here, which is observed after 42 days of submersion. After submersion in SBF, the SEM and EDS mapping of ZTA-based BG (0 to 25 wt%) composite samples are shown in Fig. 6.7 & Fig. 6.8, respectively. The microstructural investigation reveals that a thin layer of hydroxyapatite (HA) growth is observed (Fig. 6.7(a)) for the pure ZTA sample after being immersed for 42 days. Further, SEM morphology indicates that HA formation is enhanced with the BG content into ZTA after 42 days of submersion in SBF, as shown in Fig. 6.7(b-e).

Furthermore, the EDS mapping (Fig. 6.8(b-e)) confirms the presence of Ca, P, and O elements on the immersed surface of samples. The elements are the components of HA. Meanwhile, the EDS mapping of pure ZTA samples identifies only Al, Zr, Y, and O elements. Additionally, the HA layer formation over the surface of the composites is also checked by XRD analysis, and the result confirms the presence of the HA (Reference Code: 98-006-0211) phase, as shown in Fig. 6.6(c). In the XRD pattern, the intensity of the HA phase increases with the increase in BG concentration.

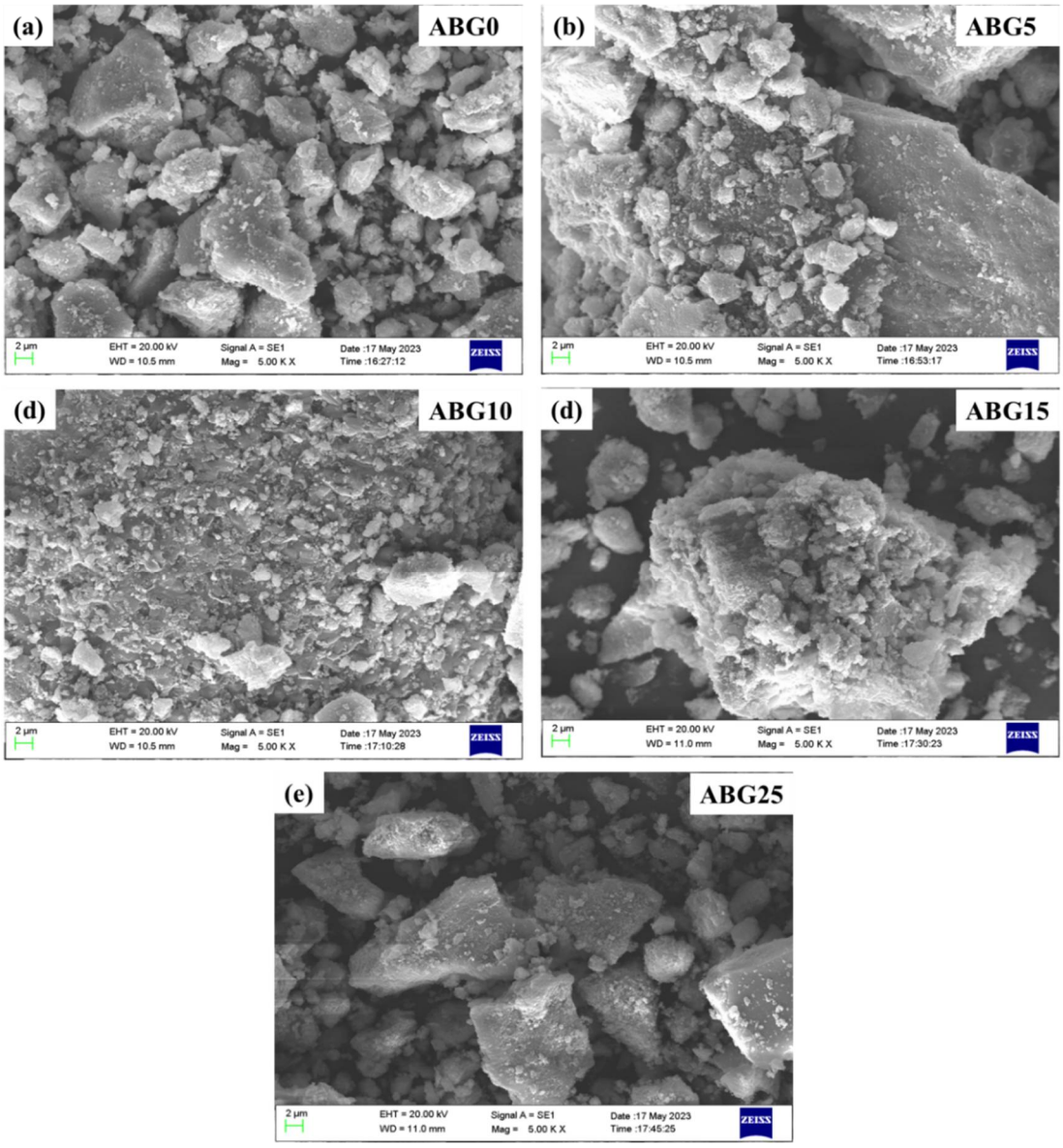

Fig. 6.7 HR-SEM of the composite samples after 42 days of immersion in SBF.

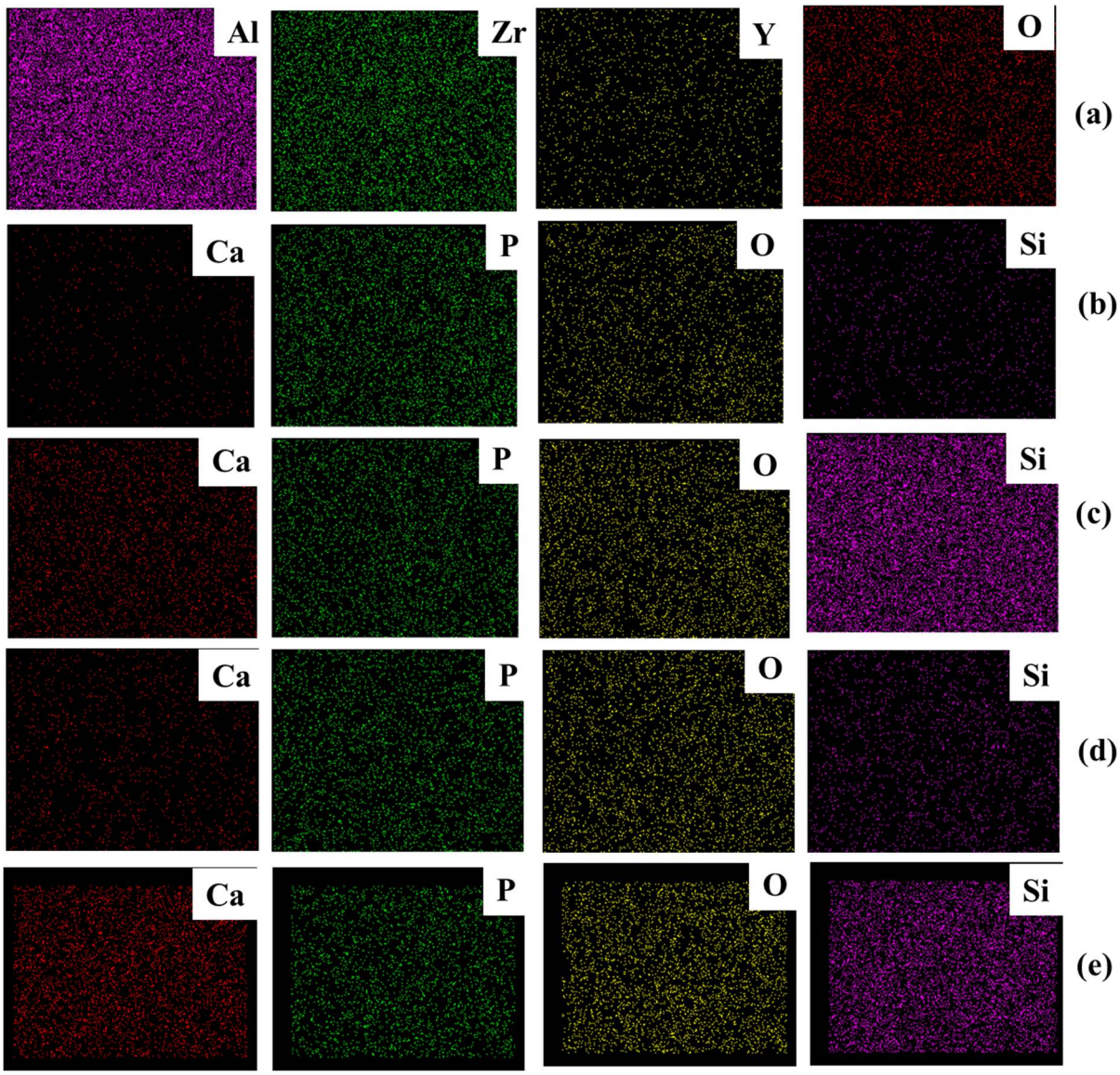

Fig. 6.8 Elemental mapping of composite samples, (a) ABG0, (b) ABG5, (c) ABG10, (d) ABG15, (e) ABG25, after 42 days of immersion in SBF.

FTIR analysis also confirms the HA formation after immersion in SBF, as shown in Fig. 6.6(d). The transmittance spectra show bands at 593, 644, 1036, 1447, 1620, 2969 and 3480 wavenumbers (cm^{-1}). The 593, 644, and 1036 cm^{-1} bands correspond to (PO_4^{-3}) (Rameshbabu *et al.*, 2005). The transmittance bands at 1447 cm^{-1} indicate the presence of carbonate ions. The 1620 and 2969 cm^{-1} bands correspond to C=O (stretch) stretching modes (Vyas *et al.*, 2015). At 3480 cm^{-1}, an OH^- band is made (Rameshbabu *et al.*, 2005) (Rameshbabu *et al.*, 2005). The intensity of the distinctive band at 1036 cm^{-1} increase with increasing BG amount, suggesting

the formation of higher HA crystallinity (Rameshbabu *et al.*, 2005). The changes in band intensity in SBF show the development and breakdown of apatite (Rameshbabu *et al.*, 2005). It is clear that when the BG content increases, the ions are emitted from the sample's surface interaction with the SBF (Sarkar *et al.*, 2019). Consequently, the circumstances leading to HA deposition increase with frequency. For the pure ZTA sample, no significant HA peak is evident, which may be due to the thin HA layer formation. The composite samples' surface-level HA production would resemble the structure of a normal BG system, where the primary site of apatite nucleation is the surface-formed hydrated silica. Subsequent to this procedure, an anionic exchange of PO_4^{3-} from SBF and the dissolution of surface-bound Ca^{2+} ions occur, resulting in the development of an HCA layer (Zhang *et al.*, 2022). As the BG addition rises, more BG particles enter into ZTA, resulting in the dispersion of Si and Ca ions. These ions help in improving the fast deposition of HA over the ZTA surface in SBF (Zhang *et al.*, 2022).

6.2.4.4 Cell culture study

6.2.4.4.1 MTT assay

The viability of osteoblast-like MG-63 cells on ZTA and ZTA-BG composites are represented in Fig. 6.9. The cell viability of all the samples (ABG0, ABG5, ABG10, ABG15, and ABG25) is enhanced with increasing the incubation time (3, 5, and 7 days of culture) and also with BG content. The surfaces of ZTA-BG composites have been found to exhibit outstanding cell viability as compared to pure ZTA samples. The cell viability of ABG5, ABG10, ABG15, and ABG25 samples is around 119, 124, 128, and 132%, respectively, after 3 days of culture. However, after 5 and 7 days of culture, the viabilities are improved by 103, 107, 115, and 124 % and 106, 113, 116, and 122 %, respectively, with respect to the pure ZTA (ABG0) sample. The enhancement of optical density (O.D.) of the entire sample (ABG0,

ABG5, ABG10, ABG15, and ABG25) as compared to the control sample is observed [represented as (*) in Fig. 6.9].

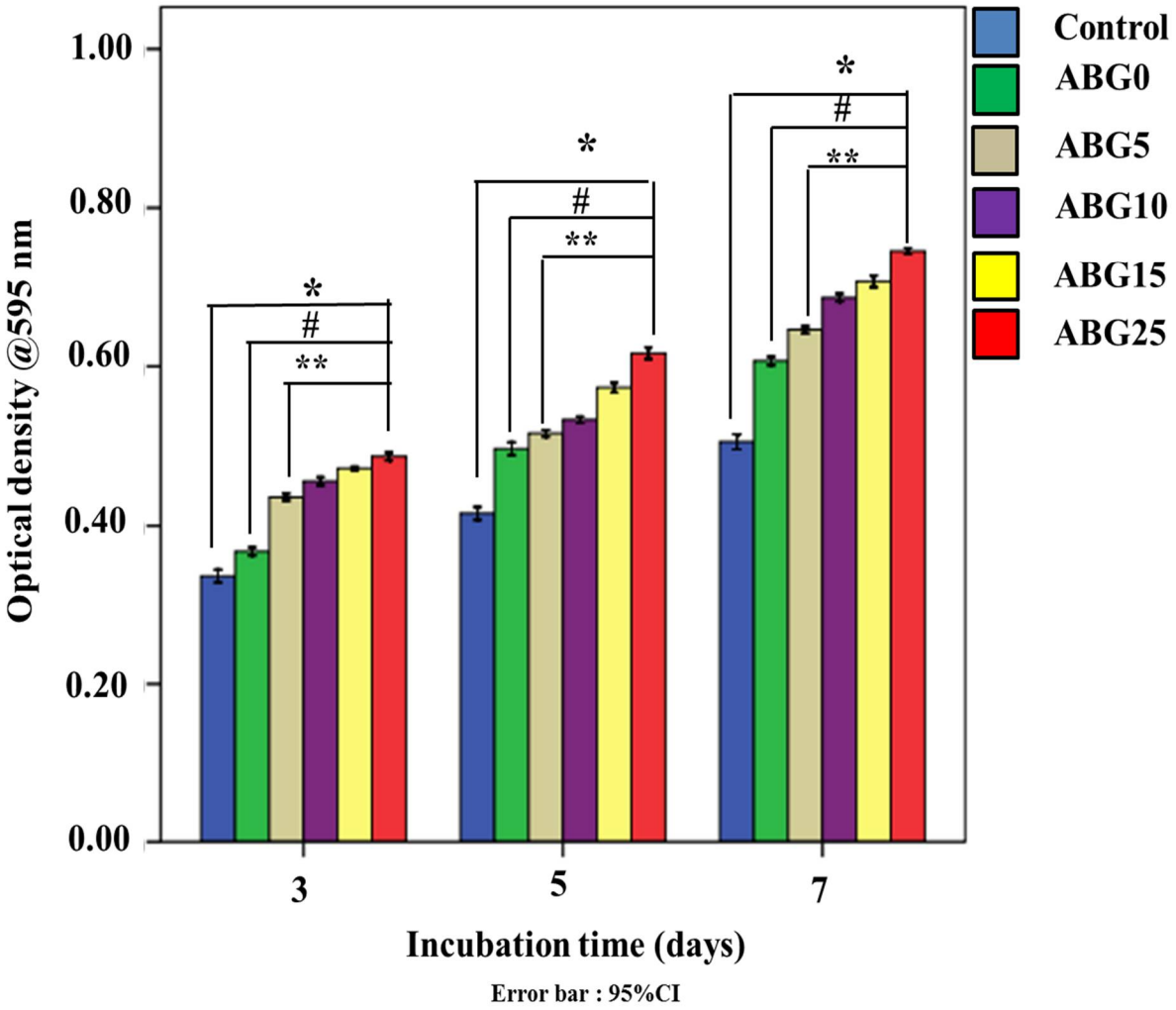

Fig. 6.9 MTT assay result for ZTA/13-93 BG bioceramic composite cultured with MG-63 cells for 3, 5, and 7 days. The symbol '*' represents the statistically significant difference in the mean optical density for all samples compared to the control sample, and '#' represents the statistically significant difference in the mean optical density for all bio-composite samples compared to the base samples ABG0. '**' represents the statistically significant difference in the mean optical density for ABG10, ABG15, and ABG25 samples compared to the ABG5 sample.

The O.D. of ABG5, ABG10, ABG15, and ABG25 samples have significantly improved compared to the ABG0 sample [represented as (#) in Fig. 6.9]. Furthermore, the O.D. of ABG10, ABG15, and ABG25 samples are significantly improved compared to the ABG5 sample [represented as (**) in Fig. 6.9]. The results show that the addition of BG to ZTA ceramic enhances cell growth, which is further confirmed by fluorescence microscopy analysis, as shown in Fig. 6.10. Composite samples ZTA-BG release ions ($Ca^{2+,}$ PO_4^{-3}, and Si^{4+}) into the incubation media during *in-vitro* cell culture, resulting in a silicon-rich surface on the composite samples (Hoppe *et al.*, 2011). Simultaneously, an efficient negative charge is generated, facilitating the absorption of proteins in the culture medium and promoting cellular growth (Hoppe *et al.*, 2011). In conclusion, it is evident that the addition of 13-93BG (0 to 25 wt%) to pure ZTA ceramic can significantly improve the cellular response of the composite.

6.2.4.4.2 Fluorescence microscopy study

The morphology of MG-63 cells, adhered to ZTA and ZTA-based composites, is studied with fluorescent microscopy [Fig. 6.10]. The findings indicate that, compared to the ABG0, the composite samples (ABG5, ABG10, ABG15, and ABG25) have better cell densities on their surfaces. The O.D. of MG-63 cells on the surface of the ZTA-BG composite is increased with the BG content. Additionally, the adhesion of MG-63 cells on the ABG0 sample's surface is flatter than that of the control. Furthermore, the density of cells increases in ABG5, ABG10, ABG15, and ABG25 samples when the BG concentration rises compared to a pure ABG0 sample. The ABG25 sample shows the highest cell density as compared to ABG0. According to reports, the ZTA is bio-inert and fails to encourage cellular viability (Zhang *et al.*, 2022). Furthermore, the BG improves the capacity of bio-insert ceramics to stimulate cell growth in bioceramic composites (Dehestani *et al.*, 2012). Ions released by BG stimulate angiogenesis, osteoblast development, and growth of cells (Verma *et al.*, 2020). The cellular and skeletal

components of bone building and metabolism are called osteoblasts (Valerio *et al.*, 2004). Because of the ionic exchange-induced release of salicylic acid from BG, the culture media possess an alkaline nature, which may be harmful to cells (Xynos *et al.*, 2000) (Silver *et al.*, 2001) (Bosetti *et al.*, 2003). Conversely, there is an increase in osteoblast viability and proliferation. This is consistent with a prior study that found a connection between alkalinization and the growth of osteoblasts (Vrouwenvelder *et al.*, 1992). Furthermore, it has been shown that the cell membrane contains voltage-activated calcium channels (Valerio *et al.*, 2004) (Gorustovich *et al.*, 2002) (Yamagushi *et al.*, 1989); moreover, alkalinization increases channel sensitivity, allowing calcium entrance into cells (Rhee *et al.*, 2003) (Seaborn *et al.*, 2002). The current data are in good accord with the increased prevalence of BG-generated ionic compounds in the media.

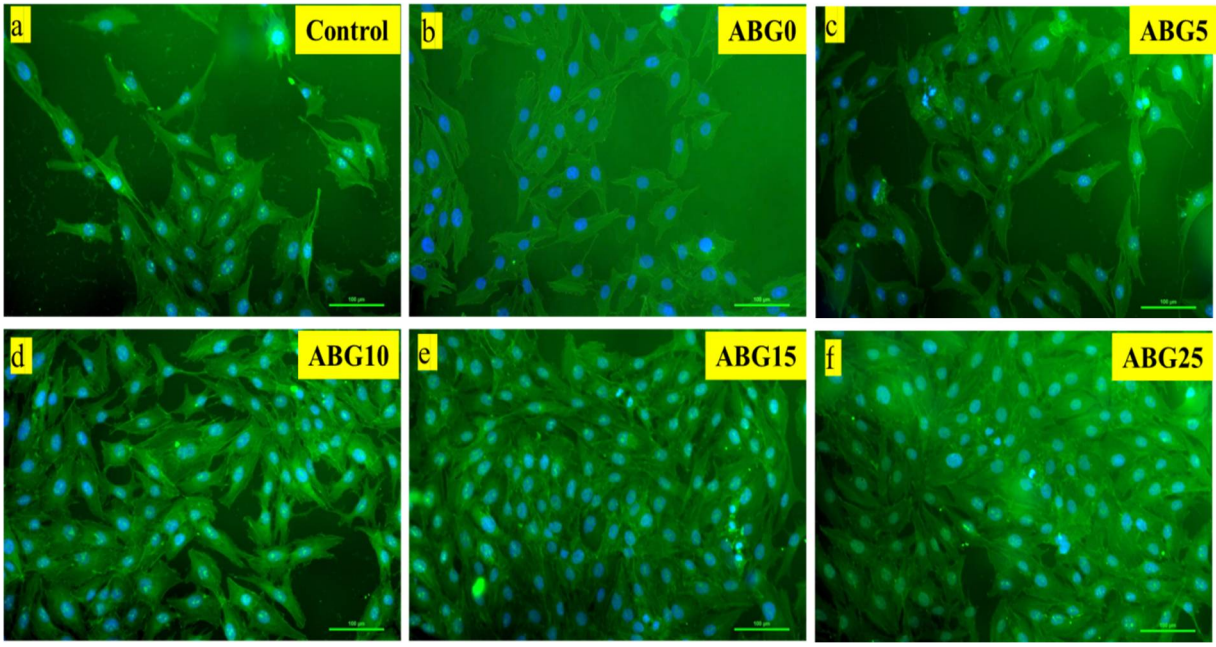

Fig. 6.10 Florescence microscopy images of MG-63 cells, adhered on the surface of ZTA/13-93 BG (0 to 25 wt% of BG) bioceramic composites, cultured for 48 h, (A) Control, (B) ABG0, (C) ABG5, (D) ABG10, (E) ABG15, and (F) ABG25. The scale bar represents 100 µm.

6.2.4.5 Antibacterial analysis

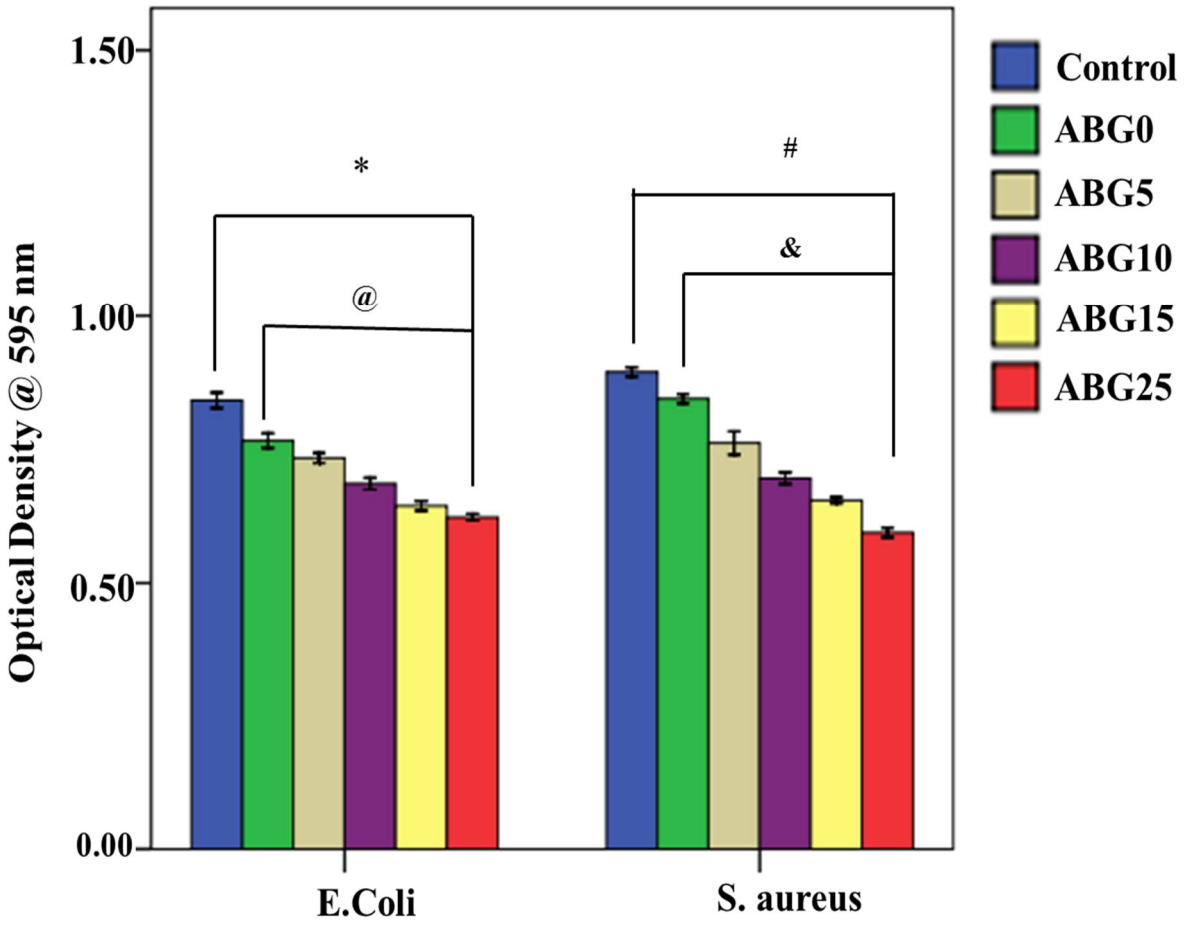

Fig. 6.11 Antibacterial response of ZTA and ZTA–xBG (x = 0, 5, 10, 15 and 25 wt%) composite for gram-negative (E. coli) and gram-positive (S. aureus) bacteria. Asterisks (*) and (#) represent the statistically significant difference among all the samples with respect to control for gram-negative (E. coli) and gram-positive (S. aureus) bacteria, respectively, at $p \leq 0.05$. Asterisks (@) and (**&**) represent the statistically significant difference among the composite samples (ABG5, ABG10, ABG15, and ABG25) with respect to the ZTA sample (ABG0) for gram-negative (E. coli) and gram-positive (S. aureus) bacteria, respectively at $p \leq 0.05$.

Fig. 6.11 shows the variation in mean O.D. of ZTA and ZTA –xBG (x = 0, 5, 10, 15, and 25 wt%) composite systems against E. coli and S. aureus bacteria. The mean O.D. for both E.

coli and S. aureus bacteria cells reduces with the addition of BG. Asterisks (*) and (#) represent the significant difference among all the samples with respect to control for E. coli and S. aureus bacteria, respectively [Fig. 6.11]. Asterisks (@) and (**&**) represent the significant difference among the composite samples (ABG5, ABG10, ABG15, and ABG25) with respect to the ZTA sample (ABG0) for E. coli and S. aureus bacteria respectively at $p \leq 0.05$ as shown in Fig. 6.11. ZTA –xBG composites decrease the mean O.D. significantly for S. aureus bacteria compared to ZTA [Fig. 6.11]. On the surfaces of ABG25, the density of S. aureus bacterial cells decreased by about 30%. The live/dead ratio of ZTA and ZTA –xBG (x = 0, 5, 10, 15, and 25 wt%) composite systems is calculated against E. coli and S. aureus bacteria with the help of O.D. of the samples. It is found that the live/dead ratio for E. coli and S. aureus bacterial cells decreases significantly with the addition of BG into ZTA. The live/dead ratio for E. aureus of ABG0, ABG5, ABG10, ABG15, and ABG25 are 10.21, 6.78, 4.42, 3.26, and 2.85, respectively. The live/dead ratio for S. aureus of ABG0, ABG5, ABG10, ABG15, and ABG25 are 16.85, 5.77, 3.51, 2.72, and 1.97, respectively. It can be observed from the antibacterial results that the BG (x = 0, 5, 10, 15, and 25 wt%) addition to ZTA enhances the antibacterial properties of ZTA. The antibacterial properties of BG are correlated with many parameters like changes in pH, dissolution rate, changes in concentration of alkali ions in glass composition, and bacterial species (Zhang *et al.*, 2010) (Allan *et al.*, 2001) (Zehnder *et al.*, 2006). Among them, antibacterial properties are affected by the increase in the pH inside the solution (Zhang *et al.*, 2010) (Allan *et al.*, 2001) (Zehnder *et al.*, 2006). Increasing glass dissolving tendency results in higher local pH and alkali ion concentrations in the solution, improving the glass's overall antibacterial properties (Zhang *et al.*, 2010) (Allan *et al.*, 2001) (Zehnder *et al.*, 2006). In this study, in-vitro biomineralization results show that the pH and degradation rate of composite samples containing BG is increased with enhancing the BG concentration. This pH and degradation rate may help to improve the antibacterial properties of the ZTA –xBG composite.

Another reason for improving antibacterial response is the presence of MgO in the BG composition. The MgO addition improves the antibacterial response of ZTA (Stoor *et al.*, 1998) (Taeh *et al.*, 2022)

6.3 Summary

In this study, the biocomposite (ZTA-BG) materials are synthesized. The mechanical properties, *In-vitro* biomineralization, and biological response of the composites are evaluated. The mechanical properties and relative density indicate that the BG content considerably impacts both. The relative density is decreased with enhancing the BG content except for a sample containing a high amount of BG (25 wt%). The flexural strength and hardness are increased with the BG additive up to 25 wt%. The *in-vitro* bioactivity, degradation, cell culture, and antibacterial of the ZTA-BG composite indicate that both are increased by enhancing the 13-93 BG content up to 25 wt%. Finally, the experimental results suggest that the ZTA-BG composite could be a feasible option for biomedical applications.

Table 6.2 Comparison of 3 biocomposites (3Y-TZP/BG, 8Mg-PSZ/BG, and ZTA/BG).

S. No.	Properties (best results)	3Y-TZP/BG	8Mg-PSZ/BG	ZTA/BG
1.	Bulk density (gm/cc)	5.93 ± 0.08	5.48 ± 0.06	4.43± 0.5
2.	Relative density	97.01±1.0	91.33 ± 0.9	89.84± 0.7
3.	Hardness (GPa)	9.0 ± 1.2	3.87 ± 1.0	3.02±1.0
4.	Flexural strength (MPa)	397. 9 ± 41.8	420 ± 32	197±18
6.	*In-vitro* bioactivity	Improved bioactivity	Improved bioactivity	Improved bioactivity
7.	Cellular viability enhanced with the addition of BG after 3 days as compared to pure matrix	134, 144, 150, and 150% corresponding to ZBG5, ZBG10, ZBG15 and ZBG25	113, 125, 126, and 128%, corresponding to MBG5, MBG10, MBG15 and MBG25	119, 124, 128, and 132%, corresponding to ABG5, ABG10, ABG15 and ABG25

The enhanced performance of all three composites (3Y-TZP/BG, 8Mg-PSZ/BG, and ZTA/BG) samples have been explained by the variations in structural, mechanical, and biological, behavior. Based on density, mechanical properties, and biological properties results, these three composites (3Y-TZP/BG, ZTA/BG, and 8Mg-PSZ/BG) are compared, as shown in Table 6.2, and found that the 3Y-TZP/BG composites have the best result. Further, machinability and tribological studies are performed on 3Y-TZP/BG composite samples only.